Performance evaluation of a dual-piezoelectric-beam vibration energy harvester with a lever and repulsive magnets

To cite this article before publication: Kai Yang *et al* 2020 *Smart Mater. Struct.* in press https://doi.org/10.1088/1361-665X/ab83ce

Performance evaluation of a dual-piezoelectric-beam vibration energy harvester with a lever and repulsive magnets

Kai Yang[1], Kewei Su[1], Junlei Wang[2,4*], Fei Wang[3], Guobiao Hu[4], Oleg Gaidai[5]

1. School of Aerospace Engineering, Huazhong University of Science and Technology, Wuhan 430074, China

2. School of Mechanical and Power Engineering, Zhengzhou University, Zhengzhou 450000, China

3. School of Microelectronics, Southern University of Science and Technology, Shenzhen 518055, China

4. Department of Mechanical Engineering, University of Auckland, 20 Symonds Street, Auckland 1010, New Zealand

5. Jiangsu University of Science and Technology, Zhenjiang 212003, China

*Corresponding author, Email: jlwang@zzu.edu.cn

ABSTRACT

This study proposes a novel dual-piezoelectric-beam vibration energy harvester with a lever and repulsive magnets (DPBLM-VEH) for performance improvement. The DPBLM-VEH integrates the benefits of the dual-beam configuration, the leverage effect and the magnetic nonlinear behavior. First, a theoretical model of the DPBLM-VEH is developed. It is found that the energy harvester exhibits two resonances in the low-frequency band, where the high-efficiency energy harvesting can be realized. A parametric study is then performed to understand the effects of various system parameters on the energy harvesting performance. Detailed design strategies in terms of tuning the lever length ratio, lever mass ratio, tip mass ratio and internal resistor towards system optimization have been proposed. Subsequently, an experimental study is conducted for validating the theoretical predictions. Experimental results show that compared to the conventional dual-piezoelectric-beam vibration energy harvester (DPB-VEH), introducing a lever (i.e., DPBL-VEH) can amplify the peak powers of the 1st and 2nd beams, respectively, by 225.8% and 134.1% around the second resonance. Similarly, the DPBLM-VEH with a further introduction of the magnetic nonlinearity can realize an amplification by 204.8% and 119.8% for the two beams. In addition, compared to the DPBL-VEH, the DPBLM-VEH can further broaden the effective bandwidths of the two beams by 98.0% and 50.6%, respectively. Therefore, we can conclude that due to the leverage effect and magnet-induced nonlinearity, the DPBLM-VEH can significantly enhance the energy conversion efficiency and broaden the operation bandwidth.

Keywords: energy harvesting; dual piezoelectric beam; magnet-induced nonlinearity; lever

1 Introduction

Energy harvesting from ambient vibrations is a promising technology that can be applied in many industrial fields [1-5]. For example, the buoy vibration energy harvesters were proposed to transduce the low-frequency ocean wave vibration into electricity [6, 7]. The beam structure with a bluff body was investigated to harvest the flow-induced vibration under wind excitations [8-12], providing a new efficient way for wind electricity generation. The electromagnetic energy harvesters were used to harvest the vibrations induced by the railway cars [13, 14], vehicle suspension systems [15, 16], aerospace vehicles [17] and human motion [18, 19]. As a result, vibration energy harvesting has received significant research interests in recent decades.

Piezoelectric beam is a typical design of energy harvester that can convert structural vibrations into electrical energy using the piezoelectric effect mechanism [20-26]. A linear piezoelectric beam is only effective and can produce considerable power output in a very narrow band around its first-mode resonance [27]. Thus, to improve the energy harvesting performance of the piezoelectric beams (widening the bandwidth and/or increasing the power output), researchers introduced magnet-induced nonlinearity into the piezoelectric-beam energy harvesters [28-34]. Tran et al. [28] comprehensively reviewed a series of piezomagnetoelastic energy harvesters and arrived at the conclusion that magnet-induced nonlinearity has been widely utilized for enhancing vibration energy harvesting performance. For example, Erturk and Inman [29] investigated a bistable non-resonant piezomagnetoelastic energy harvester that consists of a ferromagnetic cantilever and two permanent magnets. Experiment results show that the power output of the magnet-induced nonlinear piezoelectric energy harvester is increased compared to the linear counterpart. Huang et al. [30] proposed a tri-stable piezoelectric beam vibration energy harvester using magnet-induced nonlinearity of multiple magnets. The results show that the tri-stable nonlinear energy harvester can generate higher energy output over a wider range of frequency than the linear one. Zhou et al. [31] utilized the magnet-induced nonlinearity to improve the electric power generation of a piezoelectric beam under random excitations. Cai and Harne [32] investigated the geometrical design optimization of a trapezoidal piezoelectric beam with magnet-induced nonlinearity, and found that the magnet-induced monostable nonlinearity is optimal for broadening the frequency range. Zou et al. [33] conducted performance comparison of three piezoelectric beams with different arrangements of the magnets. It has been found that a reasonable arrangement of multiple magnets can reduce the threshold excitation intensity for effective energy harvesting and increasing the generated power. Rezaei et al. [34] comprehensively investigated the magnetostatic nonlinearity for performance improvement of an acoustic piezoelectric energy harvester, which validated that the introduced magnetic restoring force can effectively broaden the acoustic energy harvesting bandwidth. These literatures corroborate that by appropriately adjusting the magnet-induced nonlinearity, the energy harvesting performance of the piezoelectric beams can be significantly enhanced.

On the other hand, apart from the means of introducing magnet-induced nonlinearity, other researchers attempted to add degrees of freedom (DOF) to enhance the energy harvesting performance of the piezoelectric beam. Consequently, performance of the different types of dual-piezoelectric-beam vibration energy harvesters (DPB-VEH) were investigated [35-42]. For example, Hu et al. [35] theoretically predicted the advantages of a DPB-VEH with structural stoppers in not only widening the bandwidth but also increasing the power output. Xiong et al. [36] discovered that the 2:1 internal-resonance phenomenon can significantly widen the bandwidth of a nonlinear dual-piezoelectric-beam vibration energy harvester. Zhou et al. [37], Sun and Peter [38], Wu et al. [39, 40] corroborated that the dual-piezoelectric-beam structural configuration is beneficial to increasing the bandwidths of high vibration transmissibility (i.e., effective energy harvesting bandwidth) due to the dynamic couplings between the two beams. Xie et al. [41] presented a magnetically coupled asymmetric mono-stable dual-cantilever piezoelectric energy harvester. The dynamic coupling between the two beams improved the energy harvesting performance subjected to band-limited Gaussian white noise. It is seen that the dual-piezoelectric beam vibration energy harvester exhibits multiple resonance areas in a broad frequency band, where a large vibration transmissibility can be realized. Thus, the configuration of the dual-piezoelectric beam vibration energy harvester improves the adaptability of harvesting the vibration energy at various frequencies (which may be far away from each other in the frequency domain).

To further improve the vibration amplification in the resonance area of the dual-piezoelectric-beam vibration energy harvester, coupling a lever (which is constituted of a lever rod, supporting mass and pivot) may be an effective approach. The leverage effect can amplify the excitation, resulting in a vibration enhancement. Recently, the benefit of a lever for performance improvement of a single-degree-of-freedom (SDOF) energy harvester was validated by Wei and Jing [43] and the authors' previous studies [44, 45]. It is discovered that the leverage effect introduces an amplification factor into the excitation term. Thus, the vibration can be amplified for energy harvesting performance improvement. Though the advantage of the lever for a SDOF energy harvester has been confirmed in Refs. [43-45], the benefit of the lever for a DPB-VEH still remains unexplored. Since the DPB-VEH is a 2DOF structure (when only considering the fundamental mode of each beam) permitting energy exchange between the two DOFs, the DPB-VEH would exhibit very different dynamic behavior from the SDOF energy harvester coupled with a lever. As a result, it is worth investigating the potential of a lever for energy harvesting performance enhancement of the DPB-VEH.

Enlightened by the advantages of the magnet-induced nonlinearity, dual-piezoelectric-beam structural configuration and lever, we are motivated to combine them together to propose a novel vibration energy harvester: dual-piezoelectric-beam vibration energy harvester with a lever and repulsive magnets (DPBLM-VEH). The DPBLM-VEH consists of two piezoelectric beams placed in series, where the bottom beam is coupled with a lever structure and magnetostatic nonlinearity. The DPBLM-VEH intends to improve energy harvesting performance by broadening the effective energy harvesting bandwidth and intensifying the vibration response. The dual-beam configuration is a 2DOF structure when only considering the fundamental mode of each beam, and it thus forms two resonance modes. Both resonance modes can be employed for vibration energy harvesting, which broadens the operation bandwidth. The lever introduces tunable parameters to enhance the vibration response of the energy harvester by equivalently amplifying the excitation, yielding a higher energy harvesting efficiency. In addition, magnet-induced nonlinearity also broadens the effective bandwidth of the resonance area. To verify the advantages of integrating the dual-piezoelectric-beam structural configuration, magnet-induced nonlinearity and lever, this study will perform comparative studies of the proposed DPBLM-VEH, the dual-piezoelectric-beam vibration energy harvester with only a lever (DPBL-VEH) and the DPB-VEH. Through the numerical and experimental studies, the design guideline of the DPBLM-VEH would be presented, which brings new design concepts of the piezoelectric-beam vibration energy harvester.

The rest of the paper is organized as follows. Section 2 presents the schematic of the DPBLM-VEH, and formulates the governing equations of the DPBLM-VEH under base excitation. Subsequently, a numerical investigation of the DPBLM-VEH is performed in section 3, where the results of the other two counterparts (DPBL-VEH and DPB-VEH) are provided as well for comparison. To validate the numerical findings, an experimental study is conducted in section 4 to corroborate the numerically predicted design guidelines of the DPBLM-VEH and the comparison of the DPBLM-VEH with the other two counterparts. Finally, the main findings of this study are concluded in section 5.

2 Design concept and mathematical model

2.1 Design concept and its potential applications

Fig 1 (a) and (b) show the schematic and experimental prototype, respectively, of the dual-piezoelectric-beam vibration energy harvester coupled with a lever and repulsive magnets (DPBLM-VEH). The DPBLM-VEH is horizontally mounted on a machine which generates a base excitation. The DPBLM-VEH constitutes two piezoelectric beams (denoted as the 1st beam and 2nd beam, respectively) placed in serial. Each piezoelectric beam has a tip mass, i.e., m_1 and m_2. One magnet is mounted on the tip mass of the 1st beam, and the other magnet is mounted on the frame. The two magnets repulse each other to produce a nonlinear force. x , y are the tip displacements of the 1st and 2nd beams, respectively. The tip mass of the 1st beam m_1 connects a lever through a connecting bar. The connecting bar uses a rotational bearing to connect the tip mass, and a contact pair (which allows both rotational and sliding movements) to connect the lever rod. The connecting bar can coordinate the movements of both the beam tip mass and the lever rod. The details of this connecting bar mechanism have been described in the authors' previous research [45]. The lever consists of a lever supporting mass m_a, a homogeneous lever rod (whose total mass and length are m_r and l_r, respectively) and a pivot. The distances from the pivot to m_1 and m_a are l_1 and l_a, respectively. Two piezoelectric transducers are attached on the roots of the 1st and 2nd beams to convert the structural vibration into electrical energy. Each piezoelectric transducer has an internal capacitance C_p and an internal resistor R, where R and C_p are in parallel [46, 47].

When the repulsive magnets are removed, the prototype becomes a dual-piezoelectric-beam vibration energy harvester with only a lever (DPBL-VEH). If the lever is further removed, the prototype becomes a conventional dual-piezoelectric-beam vibration energy harvester (DPB-VEH). Both the DPBL-VEH and DPB-VEH are used as the counterparts for the following performance comparisons.

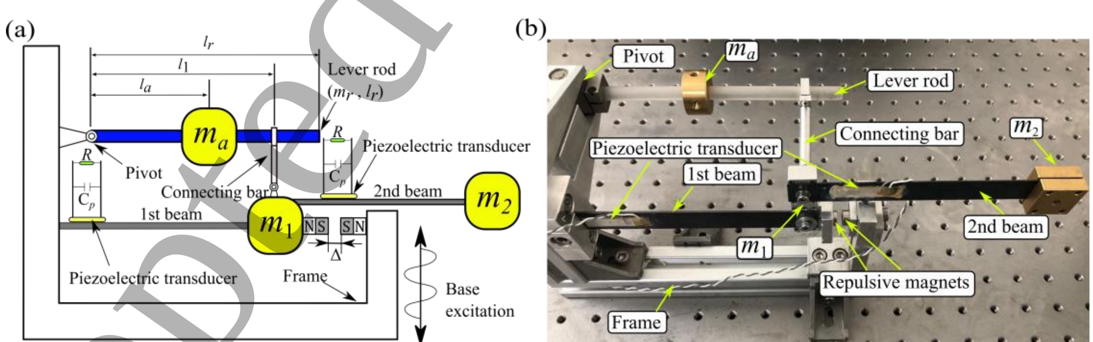

Fig 1 (a) The schematic of the DPBLM-VEH and (b) The fabricated prototype.

DPBLM-VEH is a type of mechanical vibration energy harvester, and it may have a wide application. For example, the DPBLM-VEH can be installed in a machine tool or used as a portable power generation device to harvest the vibration energy from the machine and human walking [3, 22]. Due to the various potential applications of the DPBLM-VEH, it is worth investigating its energy harvesting performance theoretically and experimentally.

2.2 Governing equations

In this study, the lever rod is assumed to be rigid and sufficiently long compared to the transverse displacement of the tip mass m_1. Hence, the lever rod's elastic deformation and influence of the rotational angle (which lead to moving direction change of m_1) are neglected. The following study assumes that the beams satisfy the planar Euler-Bernoulli beam theory, and considers only the transverse vibration. Assuming that m_1, m_2, m_a and m_r are far greater than the masses of the beams and piezoelectric transducers, the masses of the beams and piezoelectric transducers can be neglected. Therefore, the total kinetic energy of the DPBLM-VEH under the base excitation is

$$T = \frac{1}{2}m_1(\dot{x}+\dot{z})^2 + \frac{1}{2}m_2(\dot{x}+\dot{y}+\dot{z})^2 + \frac{1}{2}m_a(\alpha\dot{x}+\dot{z})^2 + \frac{1}{2}m_r\left(\frac{1}{3}\alpha_r^2\dot{x}^2 + \alpha_r\dot{x}\dot{z} + \dot{z}^2\right) \tag{1}$$

where 'over-dot' denotes derivative of the time t. z is the displacement of the base excitation. α is defined as the lever length ratio:

$$\alpha = l_a/l_1 \tag{2}$$

α_r is defined as the lever-rod length ratio:

$$\alpha_r = l_r/l_1 \tag{3}$$

The potential energy of the DPBLM-VEH is

$$V = \sum_{i=1}^{2}\left\{\frac{1}{2}EJ_i\int_0^{L_i}(w_i'')^2\mathrm{d}s - \int_{s_{pi}}^{s_{pi}+L_{pi}}\phi_p w_i'' v_i\mathrm{d}s - \frac{1}{2}C_p v_i^2\right\} + U_{mag}(x) \tag{4}$$

where $w_i(s,t)$ $(i=1,2)$ is the deformation displacement of the i^{th} beam at position s and time t. $(\,)''$ represents second order of partial differential operator $\partial^2(\,)/\partial s^2$. EJ_i is the bending stiffness of the i^{th} piezoelectric beam, which is related to the Young's modulus and the area moment of inertia of the composite structure of the beam and piezoelectric transducers. ϕ_p is the electro-mechanical transduction coefficient with respect to the piezoelectric constant and the piezoelectric transducer volume [47]. $U_{mag}(x)$ is the potential energy of the repulsive magnets based on the dipole-dipole model, which satisfies [48, 49]

$$\frac{\partial U_{mag}(x)}{\partial x} = -3Hx(x^2+\Delta^2)^{-\frac{5}{2}} \tag{5}$$

where Δ is the distance between the magnetic pole centers of the two magnets. H is the magnet feature parameter with respect to the free permeability and magnetic pole strength of the magnets. By reducing the distance Δ, the beam will be subjected to a stronger buckling force.

In this paper, the fundamental modes of both the beams are dominant and the investigated frequency is significantly smaller than the second-mode natural frequencies of both beams. This is a frequently used assumption in study of the harvester with coupled beams for exploration of the fundamental dynamic behaviors of the system according to [35, 36, 41, 42, 49], when the second-mode natural frequency of each beam is far greater than the investigated low frequency band. As a result, $w_i(s,t)$ can be approximately expressed as follows,

$$w_i(s,t) \approx \psi_i(s)q_i(t) \tag{6}$$

where $\psi_i(s)$, $q_i(t)$ $(i=1,2)$ are the fundamental mode shape function and coordinate of the i^{th} beam, respectively. Therefore, $w_1(s,t)=\lambda_1(s)x$ and $w_2(s,t)=\lambda_2(s)y$, where $\lambda_i=\psi_i(s)/\psi_i(l_i)$ $(i=1,2)$. Note that $\lambda_i \le 1$ for the fundamental-mode vibration of the i^{th} beam. By substituting $w_1(s,t)=\lambda_1(s)x$ and $w_2(s,t)=\lambda_2(s)y$ into Eq. (3), the potential energy can be rewritten as follows,

$$V = \frac{1}{2}k_1x^2 + \frac{1}{2}k_2y^2 - \Theta_1 x v_1 - \Theta_2 y v_2 - \frac{1}{2}C_p v_1^2 - \frac{1}{2}C_p v_2^2 + U_{mag}(x) \tag{7}$$

where

$$k_i = EJ_i \int_0^{l_i} (\lambda_i'')^2 \mathrm{d}s \tag{8}$$

$$\Theta_i = \int_{s_{p1}}^{s_{pi}+l_{pi}} \phi_p \lambda_i'' \mathrm{d}s \tag{9}$$

Assuming that d_i $(i = 1,2)$ is the equivalent damping coefficient of the fundamental-mode vibration of the i^{th} beam, and applying Euler–Lagrange equation, the governing equations of the DPBLM-VEH under the base excitation are derived.

$$\left(m_1 + m_2 + m_a\alpha^2 + \frac{1}{3}m_r\alpha_r^2\right)\ddot{x} + m_2\ddot{y} + d_1\dot{x} + k_1x - 3Hx(x^2 + \Delta^2)^{-\frac{5}{2}} - \Theta_1 v_1$$
$$= -\left(m_1 + m_2 + m_a\alpha + \frac{1}{2}m_r\alpha_r\right)\ddot{z} \tag{10}$$

$$m_2(\ddot{x} + \ddot{y}) + d_2\dot{y} + k_2y - \Theta_2 v_2 = -m_2\ddot{z} \tag{11}$$

where z is the base displacement. The voltage outputs of the piezoelectric transducers satisfy

$$C_p\dot{v}_1 = -\Theta_1\dot{x} - \frac{v_1}{R} \tag{12}$$

$$C_p\dot{v}_2 = -\Theta_2\dot{y} - \frac{v_2}{R} \tag{13}$$

It can be seen that Θ_i $(i = 1,2)$ are the electromechanical coupling factors, which are only related to the natural characteristics of the piezoelectric transducers and the fundamental-mode shape function $\lambda_i = \psi_i(s)/\psi_i(l_i)$. As a result, once the piezoelectric beam is manufactured, the parameter Θ_i is fixed. Usually, based on the Eqs. (12) and (13), Θ_i is identified through experiment by measuring the vibration of the beam (e.g. $\dot{x}$) and the open circuit voltage (e.g. v_1, when $R = \infty$).

Table 1 Normalized parameters and their definitions of the DPBLM-VEH

Parameter	Symbol	Definition	Parameter	Symbol	Definition
Lever length ratio	α	l_a/l_1	Normalized magnet feature parameter	β	H/m_1
Lever-rod length ratio	α_r	l/l_1	1st beam loss factor	η_1	$d_1/\sqrt{m_1k_1}$
Lever mass ratio	μ_a	m_a/m_1	2nd beam loss factor	η_2	$d_2/\sqrt{m_2k_2}$
Tip mass ratio	μ_s	m_2/m_1	1st beam characteristic frequency	ω	$\sqrt{k_1/m_1}$
Lever-rod mass ratio	μ_r	m_r/m_1	1st Piezoelectric factor	θ_1	Θ_1/m_1
Beam stiffness ratio	f	k_2/k_1	2nd Piezoelectric factor	θ_2	Θ_2/m_2

Note that according to Eq. (10), changing Δ will significantly influence the system nonlinearity. The restoring force of the 1st beam is $k_1x - 3Hx(x^2 + \Delta^2)^{-\frac{5}{2}}$, and it shows that the system will exhibit mono-stable nonlinearity (i.e., the stable static equilibrium is $x = 0$) if $\Delta \geq (k_1/3H)^{-\frac{1}{5}}$.

Eqs. (10) and (11) can be normalized as follows, where the normalized parameters and their definitions are listed in Table 1.

$$\left(1+\mu_s+\mu_a\alpha^2+\frac{1}{3}\mu_r\alpha_r^2\right)\ddot{x}+\mu_s\ddot{y}+\eta_1\omega\dot{x}+\omega^2x-3\beta x(x^2+\Delta^2)^{-\frac{5}{2}}-\theta_1 v_1 = -\left(1+\mu_s+\mu_a\alpha+\frac{1}{2}\mu_r\alpha_r\right)\ddot{z} \tag{14}$$

$$\mu_s(\ddot{x}+\ddot{y})+\eta_2\sqrt{\mu_s f}\omega\dot{y}+f\omega^2y-\mu_s\theta_2 v_2=-\mu_s\ddot{z} \tag{15}$$

3 Numerical simulation and results discussion

In this section, numerical simulations of Eqs. (12-15) under harmonic sweeping excitation are performed to demonstrate the performance enhancement of the DPBLM-VEH and reveal its dynamic behaviors. The 4th order Runge-Kutta algorithm in Matlab software is used for the following numerical simulation.

3.1 Performance comparison

Two other energy harvesters are selected for performance comparison with the proposed DPBLM-VEH. They are dual-piezoelectric-beam vibration energy harvester coupled with only a lever (DPBL-VEH) and dual-piezoelectric-beam vibration energy harvester (DPB-VEH). The DPBL-VEH is realized by removing the repulsive magnets, i.e., $\beta=0$. The DPB-VEH is implemented by further removing the lever, i.e., $[\mu_a,\mu_r,\alpha,\alpha_r]=0$. Table 2 lists the values of the simulation parameters, which are the rounded values close to the experimental prototype. By substituting the values into Eqs. (12-15) and letting all the derivatives with respect to time be zero, it is found that the static equilibrium positions are $x=0$ and $y=0$. Therefore, the DPBLM-VEH exhibits monostable nonlinearity. In the following simulations, the excitation $\ddot{z}$ is applied as a harmonic swept excitation with a constant acceleration amplitude of 6 $\mathrm{m/s^2}$ and a sweeping speed of 0.001 Hz/s.

Table 2 Values of the simulation parameters

m_1, kg	α	α_r	μ_a	μ_s	μ_r
0.08	0.6	1.2	2.0	1.1	0.3
f	η_1	η_2	ω, rad	β,	Δ, m
0.6	0.012	0.008	24π	2×10^{-8}	0.01
θ_1, N/V	θ_2, N/V	C_p, nF	R, Ω		
1.3×10^{-5}	1.7×10^{-5}	26	10^6		

Since forward harmonic sweeping excitation can easily activate the high-energy orbit responses of a nonlinear system that are beneficial to vibration energy harvesting [4, 5], the following simulation figures only present the results subjected to the forward sweeping excitation. The amplitudes of the voltage outputs v_1 and v_2 reflect the energy harvesting performance of the 1st and 2nd beams, respectively. Conventionally, the bandwidth is defined as the width of the frequency where the energy can be collected effectively. In this study, the effective bandwidth of the energy harvesting is defined as the frequency band where the voltage output is beyond 25% of the maximum value of the three harvesters' resonance peaks.

Fig 2 presents the voltage outputs of the 1st and 2nd beams of the DPBLM-VEH, DPBL-VEH and DPB-VEH under the forward harmonic sweeping excitation from 2 to 19 Hz. The curves in the figures are the envelopes of the voltage outputs. Obviously, a larger value of the voltage output indicates a better energy harvesting performance. As shown in Fig 2 (a) and (c), the three energy harvesters exhibit two resonance peaks due to the 2DOFs configuration, where the largest voltage outputs v_1 and v_2 are obtained. It should be noted that the first and second resonance in the following results have the different meanings from the modal resonant frequencies of each beam. In this study, while only the fundamental mode of each beam is considered to obtain the lumped-mass model, due to different beam configurations, the two lumped-mass models of both the beams form a two-degree-of-freedom dynamic system with different resonances as shown in governing equations Eqs. (14) and (15). Therefore, the results show the two resonance areas.

Results show that the first resonance peak is significantly larger than the second resonance peak for the 1st beam, while the voltage outputs of the first and second resonance peaks are much closer for the 2nd beam. Compared to the DPB-VEH, the first-resonance-peak voltage outputs of the 1st beam of the DPBLM-VEH and DPBL-VEH are significantly increased, while the first-resonance-peak voltage outputs of the 2nd beam are similar. This indicates that the lever is beneficial to enhancing the overall energy harvesting performance of both beams. It can be found that the enhancement of the performance is much pronounced for the second resonance due to the lever and magnet-induced nonlinearity, as shown in Fig 2 (b) and (d) which present the results of the second resonance in detail. For the three harvesters, the maximum values of the second-resonance peaks of the 1st and 2nd beams are 16.24 V and 41.65 V, respectively. Thus, the threshold voltages of defined effective bandwidth of the two beams are 4.06 V and 10.41 V($25\% \times 16.24$ V and $25\% \times 41.65$ V), respectively. The results of the second resonance area of the three harvesters are summarized in Table 3. Compared to the DPB-VEH, the second-resonance peak voltage outputs of the 1st and 2nd beams of the DPBLM-VEH are 15.69 V and 39.67 V, respectively, which are amplified by 99.9% and 170.8%. The second-resonance peak voltage outputs of the 1st and 2nd beams of the DPBL-VEH are 16.24 V and 41.65 V, respectively, which are amplified by 106.9% and 184.3%. The results indicate that integrating the lever into the DPB-VEH can significantly enhance the energy harvesting performance of the second resonance. By comparing the DPBLM-VEH and DPBL-VEH, it is found that though the second-resonance peak voltage outputs of both the harvesters are similar, the effective bandwidths of 1st and 2nd beams of the DPBLM-VEH are significantly larger. That is, the effective bandwidths of 1st and 2nd beams of the DPBLM-VEH (12.09~12.91 Hz and 11.95~12.91 Hz) are broadened by 36.7% and 57.3%, respectively, compared to the bandwidths of the DPBL-VEH (12.59~13.19 Hz and 12.55~13.16 Hz). Therefore, the results prove that the magnet-induced nonlinearity can further improve the energy harvesting performance by broadening the effective bandwidth. Overall, the simulation results verify the advantage of the lever and magnet-induced nonlinearity for performance enhancement.

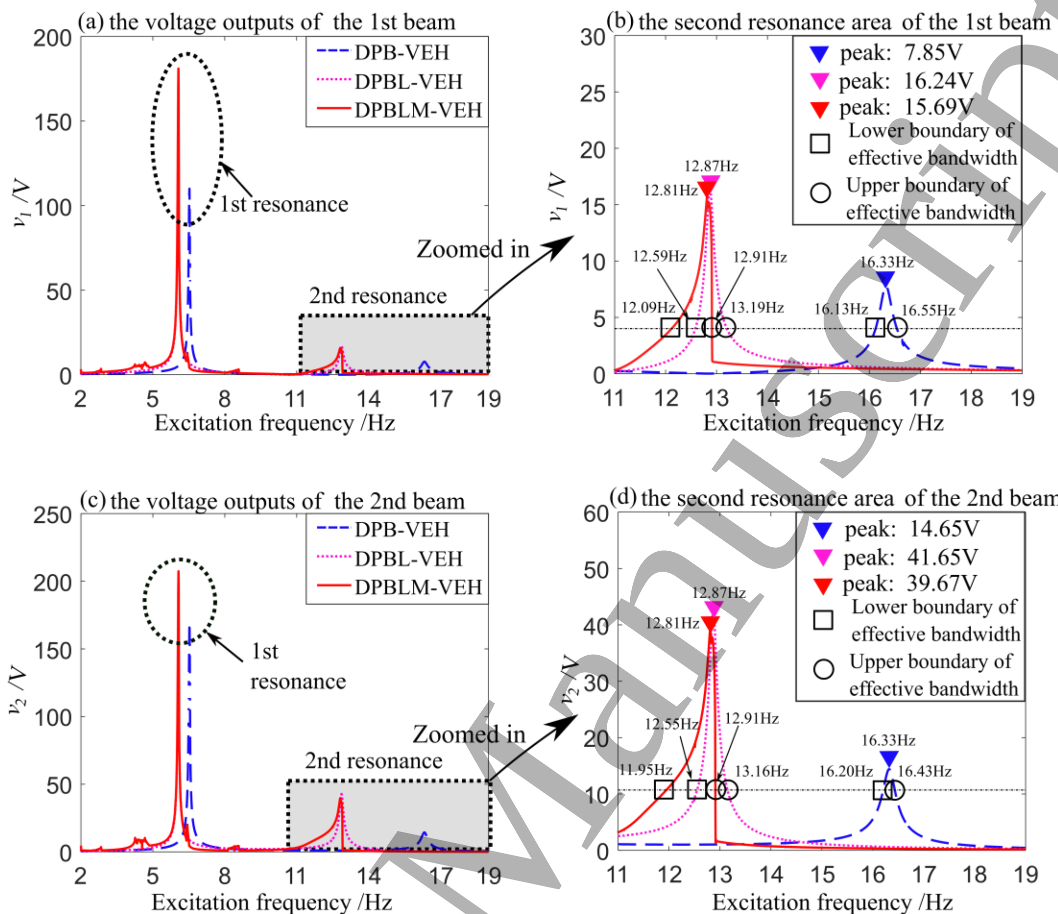

Fig 2 The voltage outputs of the DPBLM-VEH, DPBL-VEH and DPB-VEH: (a) the 1st beam; (b) the second resonance area of the 1st beam; (c) the 2nd beam; (d) the second resonance area of the 2nd beam.

Table 3 Summarized numerical results of the second resonance in Fig 2

Harvester	Beam number	Peak voltage	Effective bandwidth
DPBLM	1st beam	15.69 V	12.09~12.91 Hz
	2nd beam	39.67 V	11.95~12.91 Hz
DPBL	1st beam	16.24 V	12.59~13.19 Hz
	2nd beam	41.65 V	12.55~13.16 Hz
DPB	1st beam	7.85 V	16.13~16.55 Hz
	2nd beam	14.65 V	16.20~16.43 Hz

To understand the dynamic behaviors of the DPBLM-VEH around the second resonance, Fig 3 and Fig 4 present the dynamic responses of the 1st and 2nd beams at 12.8 Hz (the frequency close to the second resonance peak) and 13.0 Hz (the frequency where bifurcation occurs), respectively. From left to right, the three figures present the displacement response of the tip mass, the phase plot, and the fast Fourier transform (FFT) of the displacement response, respectively. As shown in Fig 3, for the 1st beam, at the excitation frequency $\omega_0 = 12.8$ Hz, the DPBLM-VEH exhibits a fundamental-periodic response, where the phase plot has a single closed loop and the FFT plot has only a single dominant frequency that equals to the excitation frequency. However, at the excitation frequency $\omega_0 = 13.0$ Hz, the DPBLM-VEH shows a multi-periodic response which is a typical nonlinear dynamic behavior. It is noted that multiple closed loops are found in the phase plot, and the FFT plot shows multiple spectrum lines: 3/11 ω_0, $4/11\omega_0$,$10/11\omega_0$ and ω_0, where $4/11\omega_0$ and ω_0 are dominant.

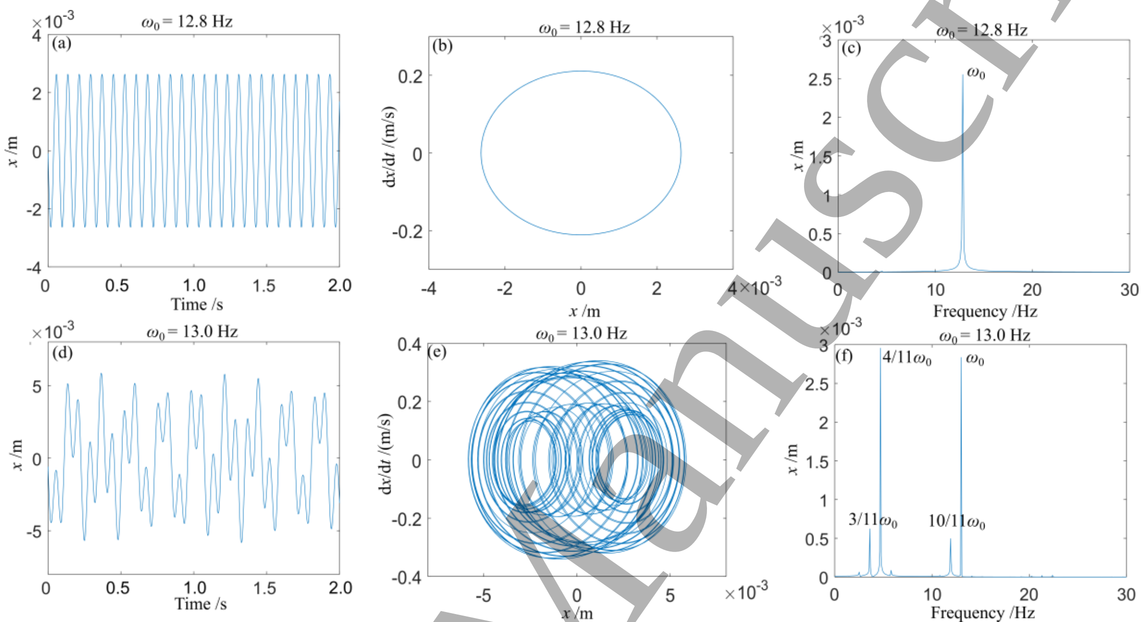

Fig 3 Dynamic responses of the 1st beam of the DPBLM-VEH at 12.8 (the top row) and 13.0 Hz (the bottom row). From left to right: (a) and (d), time series plots of the tip mass deformation displacement x; (b) and (e), phase plots of x and $\dot{x}$; (c) and (f) FFT plots of x.

Fig 4 shows that for the 2nd beam, the DPBLM-VEH also exhibits fundamental-periodic response at the excitation frequency $\omega_0 = 12.8$ Hz, and multi-periodic response at $\omega_0 = 13.0$ Hz. However, the multi-periodic response of the 2nd beam is quite distinct from that of the 1st beam at $\omega_0 = 13.0$ Hz. Three spectrum lines are found in the FFT plot: $4/11\omega_0$, $10/11\omega_0$ and ω_0. The sub-harmonic component $3/11\omega_0$ vanishes. It can be observed in Fig 3 and Fig 4 that for both the beams, when the excitation frequency is slightly greater than the frequency of the second-resonance peak, the dynamic behavior of the DPBLM-VEH changes tremendously (i.e., bifurcation).

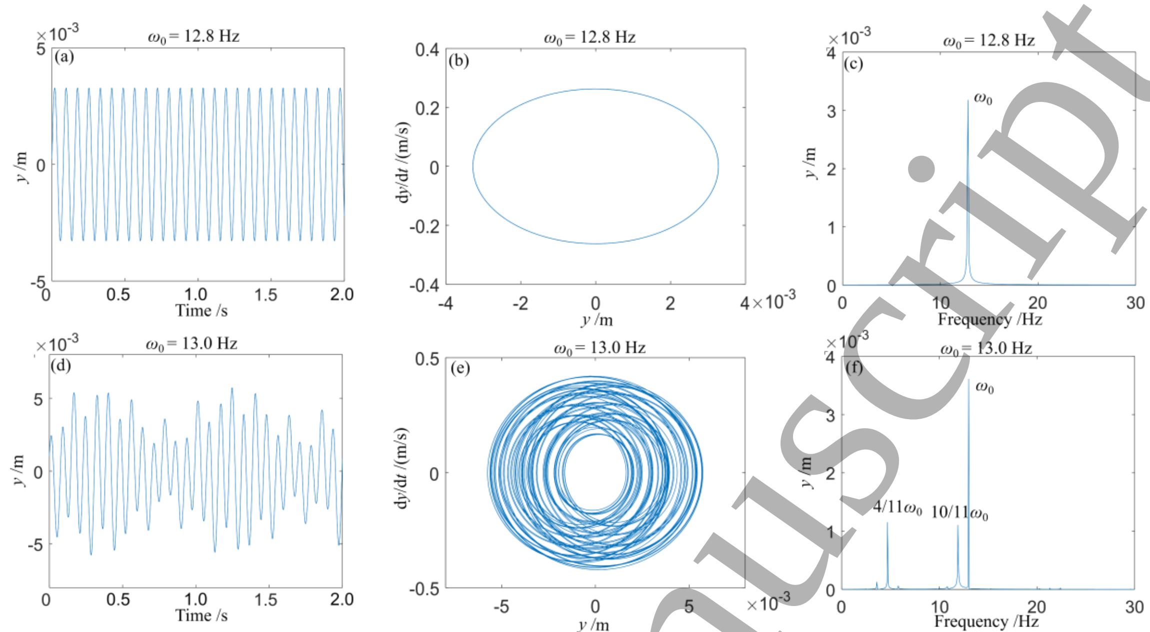

Fig 4 Dynamic responses of the 2nd beam of the DPBLM-VEH at 12.8 (the top row) and 13.0 Hz (the bottom row). From left to right: (a) and (d), time series plots of the tip mass deformation displacement y; (b) and (e), phase plots of y and $\dot{y}$; (c) and (f) FFT plots of y.

3.2 Parametric study

To give an in-depth insight into effective design of the DPBLM-VEH, a parametric study on the second resonance area is conducted to investigate the effects of various system parameters (namely, lever length ratio α, lever mass ratio μ_a, tip mass ratio μ_s, and internal resistor R) on the energy harvesting performance. In the following parametric studies, when one parameter is tuned, the others are retained as the values in Table 2.

3.2.1 Lever length ratio α

According to Eqs. (14) and (15), tuning the lever length ratio α (i.e., changing the position of lever supporting mass m_a) can vary the inertia and excitation terms, leading to the variation of the dynamic response. Results show that increasing the lever length ratio α moves both the resonance area towards the low frequency band, and variation of α influences the position of the second resonance area more significantly. Particularly, Fig 5 (b) and (d) show the second resonance voltage outputs from the 1st and 2nd beams of the DPBLM-VEH corresponding to different lever length ratios α. Based on the definition of α in Table 1 and the geometry in Fig 1, increasing lever length ratio α indicates that m_a is moving away from the pivot. As shown in Fig 5, for both the 1st and 2nd beams, the second resonance moves to the low frequency area with the increase of α. The second-resonance peak voltage output rises along with increasing α for $0 < \alpha \leq 0.7$, whereas it decreases along with increasing α for $0.7 < \alpha \leq 0.9$. This indicates that the largest voltage output (most efficient energy harvesting) can be achieved by arranging the lever supporting mass near the middle position between the lever pivot and connecting bar.

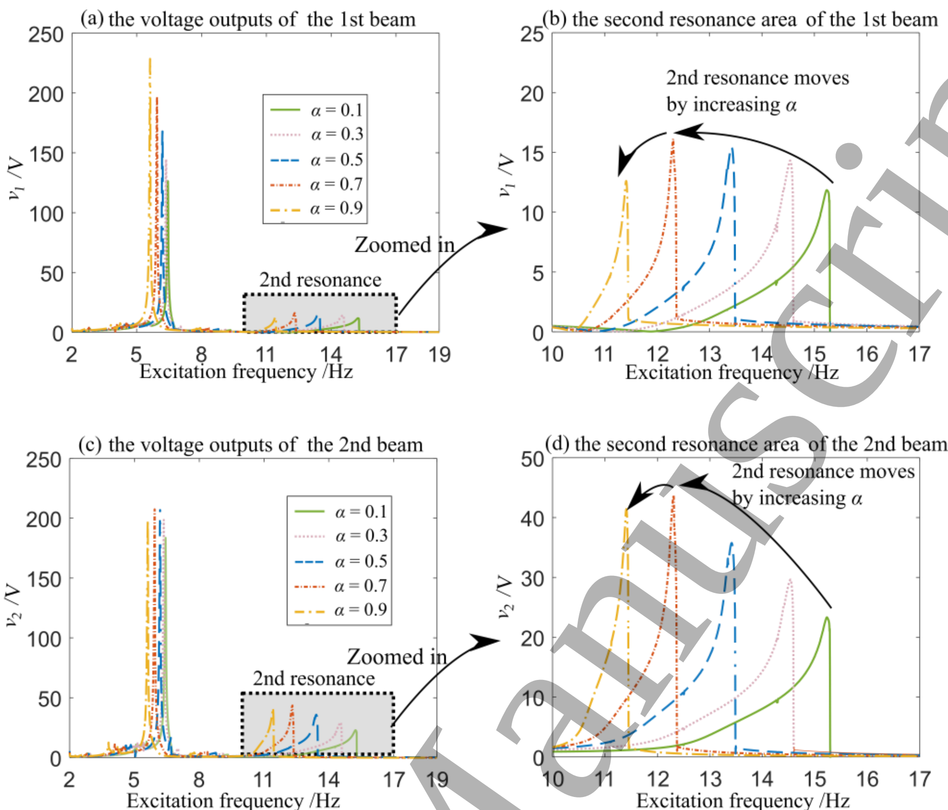

Fig 5 Voltage outputs of the (a)-(b) 1st beam and (c)-(d) 2nd beam of the DPBLM-VEH corresponding to different lever length ratios α.

3.2.2 Lever mass ratio μ_a

Fig 6 shows voltage outputs of the 1st and 2nd beams of the DPBLM-VEH corresponding to different lever mass ratios μ_a. Similar to variation of the lever length ratio α, increasing the lever mass ratio μ_a affects the position of the second resonance area more significantly, compared to the first resonance area. It can be found that for both the beams, corresponding to increase of the lever mass ratio μ_a, both the first and second resonances move towards the low frequency area, and the resonance peak voltage outputs increase. For example, the second-resonance peak voltages of the 1st and 2nd beams for $\mu_a = 3.0$ are increased by 42% and 92%, respectively, compared to $\mu_a = 1.0$. This suggests that choosing an appropriately large μ_a is beneficial to energy harvesting performance enhancement.

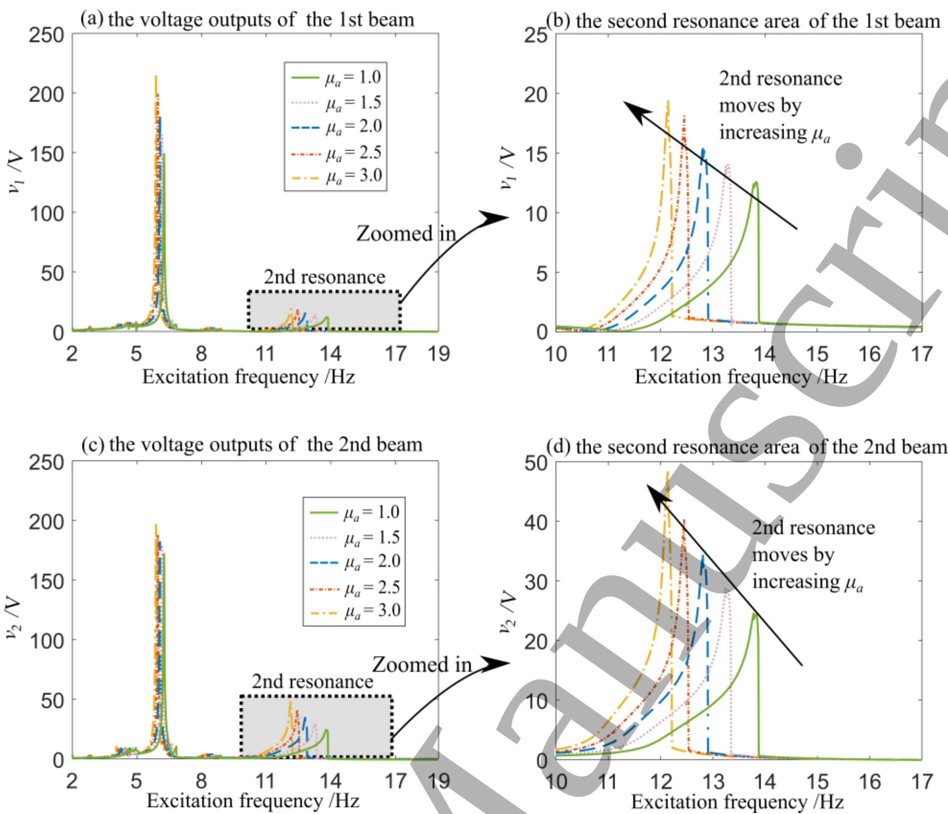

Fig 6 Voltage outputs of the (a)-(b) 1st beam and (c)-(d) 2nd beam of the DPBLM-VEH corresponding to different lever mass ratios μ_a.

3.2.3 Tip mass ratio μ_s

Fig 7 presents the voltage outputs of the 1st and 2nd beams of the DPBLM-VEH corresponding to different tip mass ratios μ_s. It is seen that both the first and second resonance areas move towards the low frequency band for the larger tip mass ratio μ_s, and increasing μ_s enhances the first-resonance peaks of both the 1st and 2nd beams. However, different variation trends of the second-resonance peaks of both the beams are observed. Corresponding to the increase of the tip mass ratio μ_s, the second-resonance peak voltage of the 1st beam rises, whereas the peak voltage of the 2nd beam declines. Thus, the results imply that certain trade-off should be considered for enhancement of the overall performance when selecting the value of the tip mass ratio.

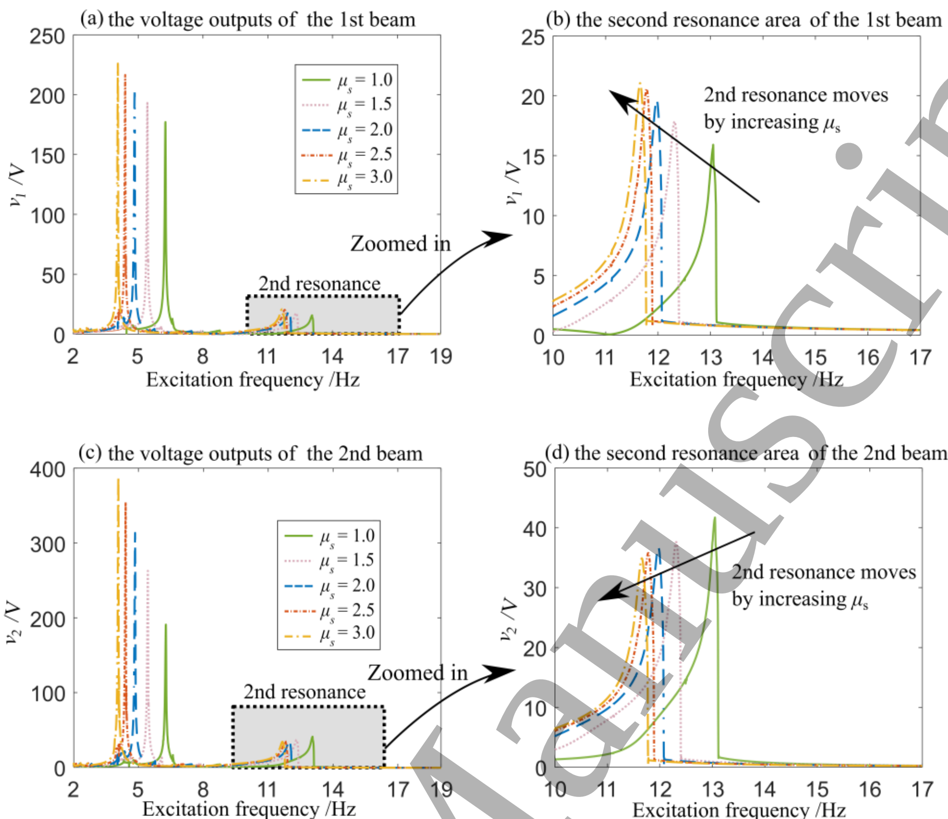

Fig 7 Voltage outputs of the (a)-(b) 1st beam and (c)-(d) 2nd beam of the DPBLM-VEH corresponding to different tip mass ratio μ_s

3.2.4 Internal resistor *R*

Fig 8 presents the voltage outputs of the 1st and 2nd beams of the DPBLM-VEH corresponding to different internal resistors *R*. It can be found that for both the beams, when increasing *R*, the positions of the first and second resonance areas are not changed, whereas the peak voltage outputs increase. Particularly in the second resonance area as shown in Fig 8 (b) and (d), the peak voltage of $R = 0.5$ MΩ is significantly higher than that of $R = 0.1$ MΩ. Although $R = 5$ MΩ is also five times of $R = 1$ MΩ, the peak voltage improvement is not as significant as the improvement of increasing $R = 0.1$ MΩ to $R = 0.5$ MΩ. This indicates that benefit of increasing *R* for voltage improvement becomes weak. Note that, the output power is defined as square of voltage output divided by the resistor *R*. On the perspective of the output power, the total output powers of both the beams corresponding to the second resonance peak are calculated: 1.318 mW for *R* = 0.1 MΩ, 2.867 mW for *R* = 0.5 MΩ, 1.572 mW for *R* = 1MΩ, 0.506 mW for *R* = 5 MΩ, and 0.278 mw for *R* = 10 MΩ. Hence, *R* = 0.5 MΩ can lead to the optimal energy harvesting in the second resonance area among the five selected resistors with respect to the given structural parameters.

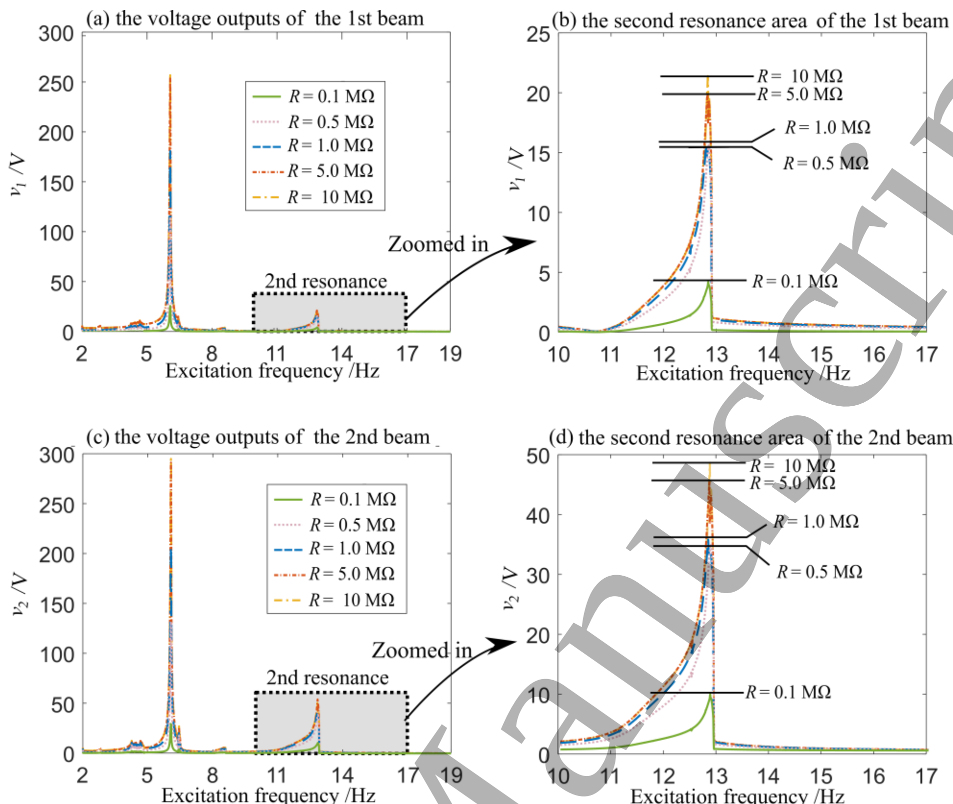

Fig 8 Voltage outputs of the (a)-(b) 1st beam and (c)-(d) 2nd beam of the DPBLM-VEH corresponding to different internal resistor R

4 Experimental validation

To validate the theoretical findings, this section performs the experimental investigation of a prototype of the DPBLM-VEH in Fig 1(b), including performance comparison and parametric studies.

4.1 Experimental setup

Fig 9 presents the experimental setup to test the performance of the DPBLM-VEH. Two identical piezoelectric transducers (material: PZT-5) are attached on the 1st and 2nd beams to convert the vibration into the electrical energy. The DPBLM-VEH is mounted on an electromagnetic shaker, which can produce up to 100 m/s^2 acceleration excitation with a frequency resolution of 0.025 Hz. An accelerometer (sensitivity: 0.2 $\mathrm{V/(m/s^2)}$) is mounted on the shaker to measure the excitation acceleration. 24-bit acquisition card NI 4497 of the NI PXIE 1082 chassis is used to acquire the output signals from the accelerometer and piezoelectric transducers. 16-bit DA card NI 6738 of the chassis is used to output the excitation signal to drive the electromagnetic shaker. Since the original voltage outputs of the piezoelectric transducers are greater than 12 V, which surpasses the limitation of the acquisition card's input range, a signal attenuator (attenuation of 10:1, internal resistor: 20 MΩ) is applied to preprocess the voltage signals of both the piezoelectric transducers.

The parameters of the piezoelectric transducers are: the capacitance is C_p= 26 nF, and the internal resistance is R =1 MΩ, which is much smaller than the resistor of the signal attenuator. As a result, the total equivalent resistor load (i.e. the parallel resistance) is approximately 1 MΩ. The geometrical parameters of each piezoelectric transducer are $30\times10\times0.4\ \mathrm{mm}^3$. The material of the two beams is China 65Mn GBT structural steel, and the geometrical parameters of the 1st and 2nd beams are $160\times19\times1.4\ \mathrm{mm}^3$ and $160\times19\times1.1\ \mathrm{mm}^3$, respectively. The tip masses of the 1st and 2nd beams are $m_1 = 0.079$ kg, $m_2 = 0.083$ kg, respectively. The mass of the lever rod is $m_r = 0.023$ kg, and its total length is $l_r = 192$ mm. The distance of the surfaces of the two repulsive magnets is tuned to be 4.5 mm, and the mutually repulsive magnets produce a magnetic repulsion force that results in only one stable equilibrium position, i.e., monostable nonlinearity. For verification of the parametric study in Section 3.2, three values of the lever supporting mass are selected: $m_a = [0.080, 0.111, 0.157]$ kg, leading to three different lever mass ratios μ_a =[1.01, 1.40, 1.98]. Three positions of the lever supporting mass on the lever rod are selected, which approximately leads to the three lever length ratios $\alpha \approx [0.4, 0.6, 0.8]$.

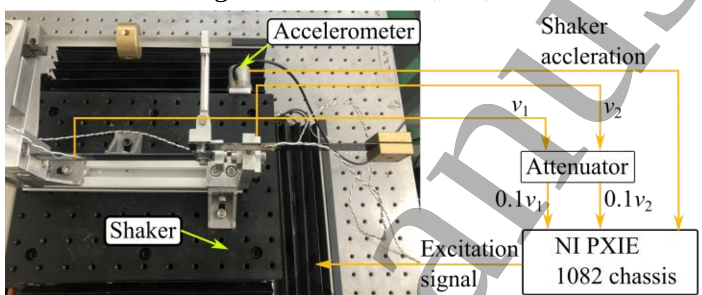

Fig 9 The experimental process

4.2 Results discussion

In the experiment, the accelerometer shows that the average excitation acceleration amplitude of the shaker is $6\ \mathrm{m/s^2}$. In the beginning, the shaker provides swept harmonic acceleration excitation from 2~19 Hz, with a sweeping speed of 0.025 Hz/s. It is observed that the DPBLM-VEH exhibits two resonance areas, where the first resonance area is approximately in 3~6 Hz and the second resonance area is in 10~16 Hz. However, the vibration displacements of both the beams in the first resonance area are tremendous, and thus the generated voltages in the first resonance area exceed the measurement limitation. On the other hand, the tremendous vibration in the first resonance area will cause the harvester to frequently strike the displacement constraint of the experimental setup. Therefore, the experimental data in the first resonance area are unable to be used for validation due to the limitation of the experimental setup. Moreover, the tremendous vibration of the harvester in the first resonance area generates the significant counter force on the shaker, which is harmful to the shaker for long-term repeatable experiment. As a result, this section only presents the experimental results in the second resonance area for verification of the numerical findings.

Fig 10 (a) and (b) present the second-resonance voltage outputs of the 1st and 2nd beams of the DPBLM-VEH under forward and backward harmonic sweeping excitations in 7~19 Hz, respectively. In this figure, lever mass ratio $\mu_a = 1.98$ and lever length ratio $\alpha \approx 0.6$. Other structural parameters are identified through the free attenuation method, which are close to the parameters for the simulation in Table 2. It can be seen that the voltage outputs of both the beams under the forward harmonic sweeping excitation are larger than those under backward sweeping excitation. This demonstrates that forward harmonic sweeping excitation can activate the high-energy orbit responses which are beneficial to energy harvesting. Therefore, the following figures only present the second-resonance experimental results of the 1st and 2nd beams.

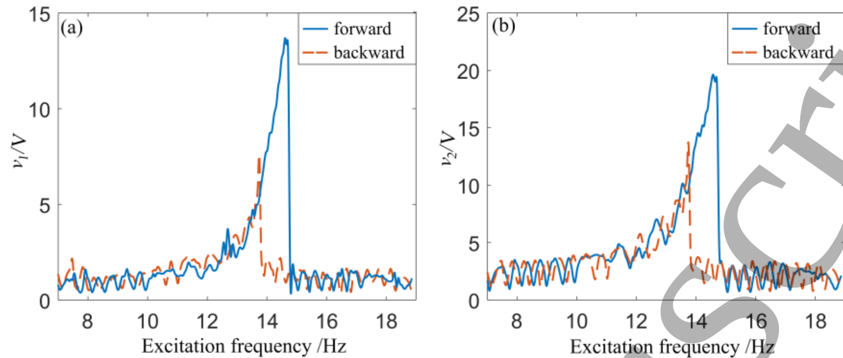

Fig 10 The experimentally measured voltage outputs of the DPBLM-VEH under forward and backward harmonic sweeping excitations in 7~19 Hz covering the second resonance: (a) the 1st beam and (b) 2nd beam.

4.2.1 Performance comparison

Fig 11 (a) and (b) present the voltage outputs of the 1st and 2nd beams of the DPBLM-VEH, DPBL-VEH and DPB-VEH in 7~19 Hz covering the second resonance area, respectively. The results show that for the two beams, both the DPBLM-VEH and DPBL-VEH outperform the DPB-VEH in the resonance peak voltage output, and the DPBLM-VEH has a wider effective bandwidth than the DPBL-VEH. Take the 1st beam as an example, the second-resonance peak voltage output of the DPBLM-VEH is 13.69 V, and the peak voltage output of the DPBL-VEH is 14.11 V. Both of them are significantly larger than that of the DPB-VEH (7.88 V). The effective bandwidth (where the voltage output is over 25% of the maximum peak voltages of the three harvesters) of the DPBLM-VEH is 11.52~14.49 Hz, which is wider than that of the DPBL-VEH (14.33~15.83 Hz). Comparing the experimental data in Fig 11 and numerical results in Fig 2 (b) and (d), it is seen that both the results validate the advantage of the lever mechanism for enhancing the second-resonance peak voltage and the benefit of the magnet-induced nonlinearity for broadening the bandwidth. Note that there exist some discrepancies between the numerical and experimental results for the DPBLM-VEH and DPBL-VEH. The discrepancies can be interpreted as follows. In the experiment, the lever's pivot and connecting bar bring the additional friction into DPBLM-VEH and DPBL-VEH, which degrades the second resonance peak. On the other hand, as shown in Fig 1 (b), the connecting bar's contact pair can slide along the lever rod during vibration. This unmodeled sliding motion may also bring the discrepancy between the experimental and numerical results. Regardless of the discrepancies, both the experimental and numerical results are in good agreement, which verifies the theoretical findings.

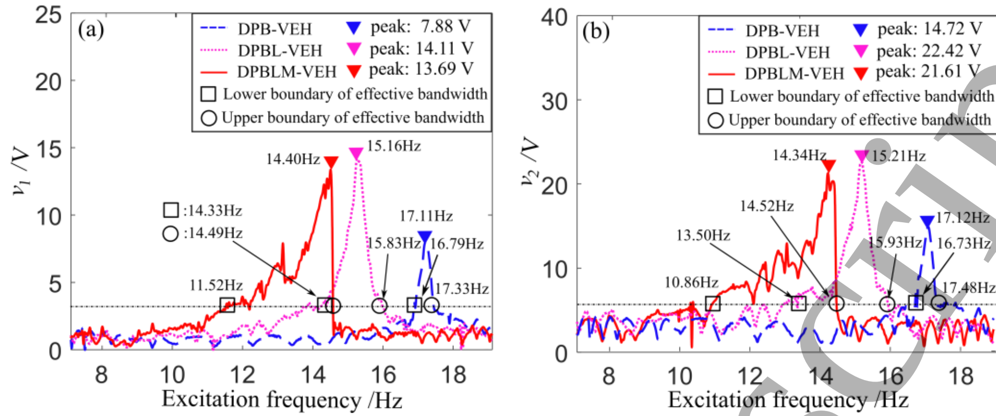

Fig 11 The experimentally measured voltage outputs of the DPBLM-VEH, DPBL-VEH and DPB-VEH in 7~19 Hz covering the second resonance area: (a) the 1st beam and (b) 2nd beam

Fig 12 (a) and (b) present the estimated power outputs of the 1st and 2nd beams of the DPBLM-VEH, DPBL-VEH and DPB-VEH in 7~19 Hz, respectively. Since the attenuator is a circuit board, each channel of which consists of a resistor $R \approx 1$ MΩ (measured by the ohm gauge), the power outputs can be calculated by $P_1 = v_1^2/R_1$ and $P_2 = v_2^2/R_2$. Based on the results in Fig 11 and Fig 12, Table 4 summarizes the second-resonance peak voltage outputs, power outputs and effective bandwidths of the 1st and 2nd beams of the DPBLM-VEH and DPBL-VEH. It can be found that compared to the DPB-VEH, the DPBL-VEH can amplify the second-resonance peak powers of the 1st and 2nd beams respectively by 225.8% and 134.1%, whereas the DPBLM-VEH can amplify the second-resonance peak power outputs respectively by 204.8% and 119.8%. In addition, DPBLM-VEH can further broaden the effective bandwidths of both the beams by 98.0% and 50.6%, respectively, compared to the DPBL-VEH which does not have the magnet-induced nonlinearity.

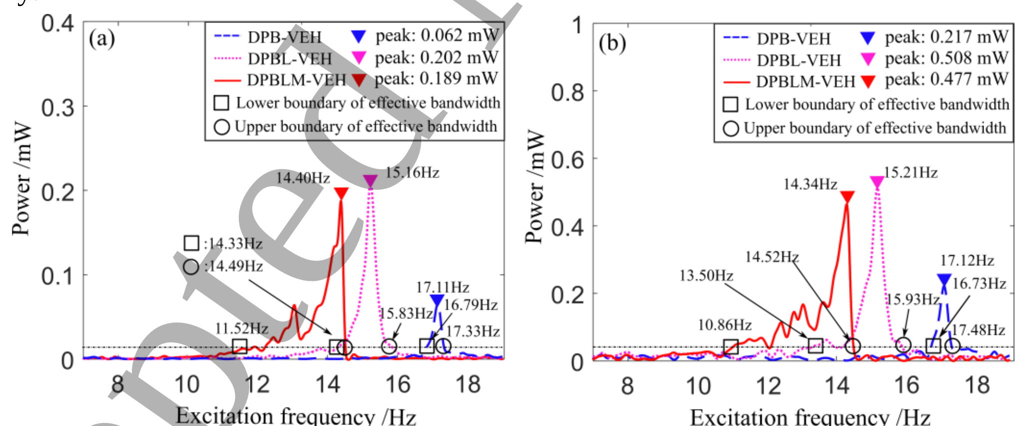

Fig 12 The estimated power outputs of the DPBLM-VEH, DPBL-VEH and DPB-VEH in 7~19 Hz covering the second resonance area: (a) the 1st beam and (b) 2nd beam

Table 4 Summarized results of the second resonance area in the experiments

Harvester	Beam number	Peak voltage	Effective bandwidth	Peak power
DPBLM	1st beam	13.69 V	11.52~14.49 Hz	0.189 mW
	2nd beam	21.61 V	10.86~14.52 Hz	0.477 mW
DPBL	1st beam	14.11 V	14.33~15.83 Hz	0.202 mW
	2nd beam	22.42 V	13.50~15.93 Hz	0.508 mW
DPB	1st beam	7.88 V	16.79~17.33 Hz	0.062 mW
	2nd beam	14.72 V	16.73~17.48 Hz	0.217 mW

4.2.2 Validation of the parametric studies

Fig 13 presents experimentally measured second-resonance voltage outputs of the 1st and 2nd beams of the DPBLM-VEH for $\alpha = [0.4, 0.6, 0.8]$ in 7~19 Hz, respectively. The results show that for both the beams, the resonance moves to the lower frequency band when α increases, and the resonance peak voltage output for the position $\alpha = 0.6$ reaches the maximum. This variation trend agrees well with the numerically predicted variation trend in Fig 5. Fig 14 presents the experimentally measured voltage outputs of the 1st and 2nd beams of the DPBLM-VEH corresponding to μ_a =[1.01, 1.40, 1.98] in 7~19 Hz, respectively. It can be found that for both the beams, increasing the lever mass ratio can improve the energy harvesting performance of DPBLM-VEH, and the second resonance area moves to the low frequency. Thus, the experimental results validate the numerical results presented in Fig 6, which indicates that a larger μ_a is favorable for energy harvesting performance.

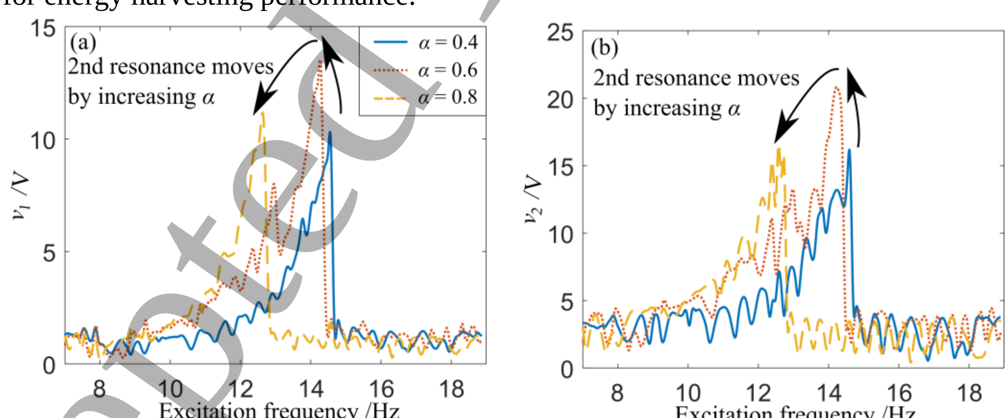

Fig 13 The experimentally measured second-resonance voltage outputs of the DPBLM-VEH for $\alpha = [0.4\ 0.6, 0.8]$ and $\mu_a = 1.98$ in 7~19 Hz covering the second resonance area: (a) the 1st beam and (b) 2nd beam

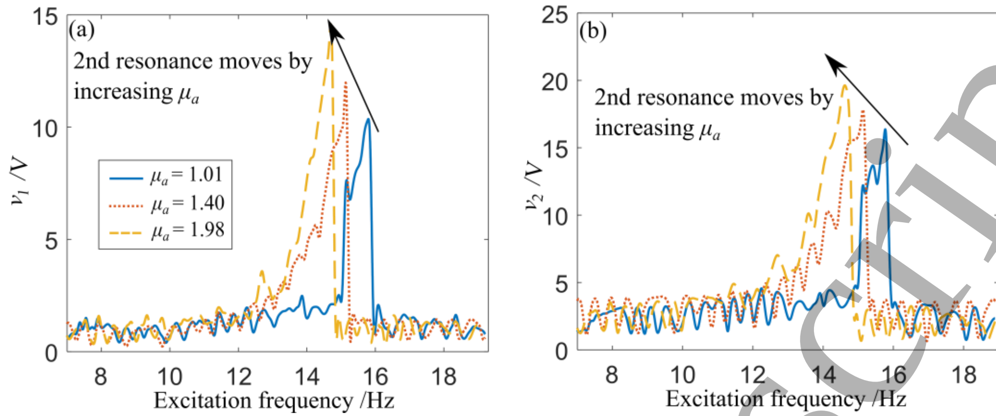

Fig 14 The experimentally measured second-resonance voltage outputs of the DPBLM-VEH for $\mu_a = [1.01, 1.40, 1.98]$ and $\alpha = 0.6$ in 7~19 Hz covering the second resonance area: (a) the 1st beam and (b) 2nd beam

5 Conclusions

This study proposes a novel vibration energy harvester: dual-piezoelectric-beam vibration energy harvester with a lever and repulsive magnets (DPBLM-VEH), which uses the lever and magnet-induced nonlinearity for amplifying the electric power and broadening the effective energy harvesting bandwidth, respectively. The DPBLM-VEH is investigated through numerical simulation and experiment, and both the numerical and experimental results have a good agreement. Results show that the DPBLM-VEH exhibits two resonances, where the peak amplitude and position of the second resonance in the frequency domain can be significantly affected by both the lever and magnet-induced nonlinearity. To verify the advantages of the DPBLM-VEH, this study conducts performance comparison of the DPBLM-VEH, the dual-piezoelectric-beam vibration energy harvester (DPB-VEH) and the dual-piezoelectric-beam vibration energy harvester with only a lever (DPBL-VEH). It is found that the DPBLM-VEH can not only significantly enhance the second-resonance peak power due to the advantage of the lever, but also broaden the effective energy harvesting bandwidth due to the magnet-induced nonlinearity. Therefore, the DPBLM-VEH significantly outperforms the other two counterparts. The parametric studies suggest that it is beneficial to energy harvesting performance of the DPBLM-VEH by arranging the lever supporting mass near the middle position between the lever pivot and connecting bar, and selecting an appropriately large lever supporting mass. In addition, the study also reveals a trade-off of the overall performance between the 1st and 2nd beams in terms of the tip mass ratio of both the beams, and uncovers that there exists an optimal value of the resistor leading to the highest output power of the second resonance area of the DPBLM-VEH.

Acknowledgements

This work is supported by National Natural Science Foundation of China (Grant No. 11802097 and 51977196).

References

[1] A.R.M. Siddique, S. Mahmud, B. Van Heyst, A comprehensive review on vibration based micro power generators using electromagnetic and piezoelectric transducer mechanisms, Energy Conversion and Management, 106 (2015) 728-747.
[2] M. Cheng, Y. Zhu, The state of the art of wind energy conversion systems and technologies: A review, Energy Conversion and Management, 88 (2014) 332-347.
[3] H.-X. Zou, L.-C. Zhao, Q.-H. Gao, L. Zuo, F.-R. Liu, T. Tan, K.-X. Wei, W.-M. Zhang, Mechanical modulations for enhancing energy harvesting: Principles, methods and applications, Applied Energy, 255 (2019) 113871.
[4] S. Zhou, J. Cao, A. Erturk, J. Lin, Enhanced broadband piezoelectric energy harvesting using rotatable magnets, Applied physics letters, 102 (2013) 173901.
[5] K. Yang, Q. Zhou, Robust optimization of a dual-stage bistable nonlinear vibration energy harvester considering parametric uncertainties, Smart Materials and Structures, 28 (2019) 115018.
[6] R. Harne, M. Schoemaker, B. Dussault, K. Wang, Wave heave energy conversion using modular multistability, Applied energy, 130 (2014) 148-156.
[7] N. Viet, Q. Wang, Ocean wave energy pitching harvester with a frequency tuning capability, Energy, 162 (2018) 603-617.
[8] J. Wang, L. Tang, L. Zhao, Z. Zhang, Efficiency investigation on energy harvesting from airflows in HVAC system based on galloping of isosceles triangle sectioned bluff bodies, Energy, 172 (2019) 1066-1078.
[9] G. Hu, J. Wang, Z. Su, G. Li, H. Peng, K. Kwok, Performance evaluation of twin piezoelectric wind energy harvesters under mutual interference, Applied Physics Letters, 115 (2019) 073901.
[10] Z. Lai, J. Wang, C. Zhang, G. Zhang, D. Yurchenko, Harvest wind energy from a vibro-impact DEG embedded into a bluff body, Energy Conversion and Management, 199 (2019) 111993.
[11] K. Yang, J. Wang, D. Yurchenko, A double-beam piezo-magneto-elastic wind energy harvester for improving the galloping-based energy harvesting, Applied Physics Letters, 115 (2019) 193901.
[12] J. Wang, S. Zhou, Z. Zhang, D. Yurchenko, High-performance piezoelectric wind energy harvester with Y-shaped attachments, Energy conversion and management, 181 (2019) 645-652.
[13] M. Gao, J. Cong, J. Xiao, Q. He, S. Li, Y. Wang, Y. Yao, R. Chen, P. Wang, Dynamic modeling and experimental investigation of self-powered sensor nodes for freight rail transport, Applied Energy, 257 (2020) 113969.
[14] Y. Pan, F. Liu, R. Jiang, Z. Tu, L. Zuo, Modeling and onboard test of an electromagnetic energy harvester for railway cars, Applied Energy, 250 (2019) 568-581.
[15] X. Xie, Q. Wang, Energy harvesting from a vehicle suspension system, Energy, 86 (2015) 385-392.
[16] M.A. Abdelkareem, L. Xu, M.K.A. Ali, A. Elagouz, J. Mi, S. Guo, Y. Liu, L. Zuo, Vibration energy harvesting in automotive suspension system: A detailed review, Applied energy, 229 (2018) 672-699.
[17] D. Li, Y. Wu, A. Da Ronch, J. Xiang, Energy harvesting by means of flow-induced vibrations on aerospace vehicles, Progress in Aerospace Sciences, 86 (2016) 28-62.
[18] K. Fan, M. Cai, F. Wang, L. Tang, J. Liang, Y. Wu, H. Qu, Q. Tan, A string-suspended and driven rotor for efficient ultra-low frequency mechanical energy harvesting, Energy Conversion and Management, 198 (2019) 111820.
[19] K. Ylli, D. Hoffmann, A. Willmann, P. Becker, B. Folkmer, Y. Manoli, Energy harvesting from human motion: exploiting swing and shock excitations, Smart Materials and Structures, 24 (2015) 025029.
[20] A. Erturk, D.J. Inman, Issues in mathematical modeling of piezoelectric energy harvesters, Smart Materials and Structures, 17 (2008) 065016.
[21] Y. Li, S. Zhou, Z. Yang, T. Guo, X. Mei, High-performance low-frequency bistable vibration energy harvesting plate with tip mass blocks, Energy, 180 (2019) 737-750.
[22] I. Izadgoshasb, Y.Y. Lim, N. Lake, L. Tang, R.V. Padilla, T. Kashiwao, Optimizing orientation of piezoelectric cantilever beam for harvesting energy from human walking, Energy Conversion and Management, 161 (2018) 66-73.

[23] M. Rezaei, R. Talebitooti, S. Rahmanian, Efficient energy harvesting from nonlinear vibrations of PZT beam under simultaneous resonances, Energy, 182 (2019) 369-380.
[24] M. Rezaei, S.E. Khadem, P. Firoozy, Broadband and tunable PZT energy harvesting utilizing local nonlinearity and tip mass effects, International Journal of Engineering Science, 118 (2017) 1-15.
[25] M. Rezaei, R. Talebitooti, Wideband PZT energy harvesting from the wake of a bluff body in varying flow speeds, International Journal of Mechanical Sciences, 163 (2019) 105135.
[26] K. Vijayan, M. Friswell, H.H. Khodaparast, S. Adhikari, Non-linear energy harvesting from coupled impacting beams, International Journal of Mechanical Sciences, 96 (2015) 101-109.
[27] M.F. Daqaq, R. Masana, A. Erturk, D. Dane Quinn, On the role of nonlinearities in vibratory energy harvesting: a critical review and discussion, Applied Mechanics Reviews, 66 (2014).
[28] N. Tran, M.H. Ghayesh, M. Arjomandi, Ambient vibration energy harvesters: A review on nonlinear techniques for performance enhancement, International Journal of Engineering Science, 127 (2018) 162-185.
[29] A. Erturk, D.J. Inman, Broadband piezoelectric power generation on high-energy orbits of the bistable Duffing oscillator with electromechanical coupling, Journal of Sound and Vibration, 330 (2011) 2339-2353.
[30] D. Huang, S. Zhou, G. Litak, Analytical analysis of the vibrational tristable energy harvester with a RL resonant circuit, Nonlinear Dynamics, 97 (2019) 663-677.
[31] Z. Zhou, W. Qin, W. Du, P. Zhu, Q. Liu, Improving energy harvesting from random excitation by nonlinear flexible bi-stable energy harvester with a variable potential energy function, Mechanical Systems and Signal Processing, 115 (2019) 162-172.
[32] W. Cai, R.L. Harne, Vibration energy harvesters with optimized geometry, design, and nonlinearity for robust direct current power delivery, Smart Materials and Structures, 28 (2019) 075040.
[33] H.-X. Zou, W.-M. Zhang, W.-B. Li, K.-X. Wei, K.-M. Hu, Z.-K. Peng, G. Meng, Magnetically coupled flextensional transducer for wideband vibration energy harvesting: design, modeling and experiments, Journal of Sound and Vibration, 416 (2018) 55-79.
[34] M. Rezaei, R. Talebitooti, F. M.I, Efficient acoustic energy harvesting by deploying magnetic restoring force, Smart Materials and Structures, 28 (2019) 105037.
[35] G. Hu, L. Tang, R. Das, P. Marzocca, A two-degree-of-freedom piezoelectric energy harvester with stoppers for achieving enhanced performance, International Journal of Mechanical Sciences 149 (2018) 500-507.
[36] L. Xiong, L. Tang, B.R. Mace, A comprehensive study of 2: 1 internal-resonance-based piezoelectric vibration energy harvesting, Nonlinear Dynamics, 91 (2018) 1817-1834.
[37] W. Zhou, G.R. Penamalli, L. Zuo, An efficient vibration energy harvester with a multi-mode dynamic magnifier, Smart Materials and Structures, 21 (2011) 015014.
[38] S. Sun, W.T. Peter, Modeling of a horizontal asymmetric U-shaped vibration-based piezoelectric energy harvester (U-VPEH), Mechanical Systems and Signal Processing, 114 (2019) 467-485.
[39] H. Wu, L. Tang, Y. Yang, C.K. Soh, A novel two-degrees-of-freedom piezoelectric energy harvester, Journal of Intelligent Material Systems and Structures, 24 (2013) 357-368.
[40] H. Wu, L. Tang, Y. Yang, C.K. Soh, Development of a broadband nonlinear two-degree-of-freedom piezoelectric energy harvester, Journal of Intelligent Material Systems and Structures, 25 (2014) 1875-1889.
[41] Z. Xie, S. Zhou, J. Xiong, W. Huang, The benefits of a magnetically coupled asymmetric monostable dual-cantilever energy harvester under random excitation, Journal of Intelligent Material Systems and Structures, 30 (2019) 3136-3145.
[42] C. Lan, L. Tang, W. Qin, L. Xiong, Magnetically coupled dual-beam energy harvester: Benefit and trade-off, Journal of Intelligent Material Systems and Structures, 29 (2017) 1216-1235.
[43] C. Wei, X. Jing, Vibrational energy harvesting by exploring structural benefits and nonlinear characteristics, Communications in Nonlinear Science and Numerical Simulation, 48 (2017) 288-306.
[44] K. Yang, F. Fei, J. Du, Investigation of the lever mechanism for bistable nonlinear energy harvesting under Gaussian-type stochastic excitations, Journal of Physics D: Applied Physics, 52 (2018) 055501.
[45] K. Yang, F. Fei, H. An, Investigation of coupled lever-bistable nonlinear energy harvesters for enhancement of inter-well dynamic response, Nonlinear Dynamics, 96 (2019) 2369-2392.

[46] J. Liang, Y. Zhao, K. Zhao, Synchronized triple bias-flip interface circuit for piezoelectric energy harvesting enhancement, IEEE Transactions on Power Electronics, 34 (2018) 275-286.
[47] A. Erturk, D.J. Inman, Piezoelectric energy harvesting, John Wiley & Sons, 2011.
[48] K. Yang, R.L. Harne, K.W. Wang, H. Huang, Investigation of a bistable dual-stage vibration isolator under harmonic excitation, Smart Materials and Structures, 23 (2014) 045033.
[49] L. Xiong, L. Tang, B.R. Mace, Internal resonance with commensurability induced by an auxiliary oscillator for broadband energy harvesting, Applied Physics Letters, 108 (2016) 203901.